Visualizing the protons in a metalloenzyme electron proton transfer pathway

Hanna Kwon[a], Jaswir Basran[b,c], Juliette M. Devos[d], Reynier Suardíaz[a,e], Marc W. van der Kamp[e], Adrian J. Mulholland[a], Tobias E. Schrader[f], Andreas Ostermann[g], Matthew P. Blakeley[h], Peter C. E. Moody[b,c,1], and Emma L. Raven[a,1]

[a]School of Chemistry, University of Bristol, Bristol BS8 1TS, United Kingdom; [b]Department of Molecular and Cell Biology, University of Leicester, Leicester LE1 7RH, United Kingdom; [c]Leicester Institute of Structural and Chemical Biology, University of Leicester, Leicester LE1 7RH, United Kingdom; [d]Life Sciences Group, Institut Laue-Langevin, 38000 Grenoble, France; [e]School of Biochemistry, University of Bristol, Bristol BS8 1TD, United Kingdom; [f]Jülich Centre for Neutron Science at Heinz Maier-Leibnitz Zentrum, Forschungszentrum Jülich GmbH, 85748 Garching, Germany; [g]Heinz Maier-Leibnitz Zentrum, Technische Universität München, D-85748 Garching, Germany; and [h]Large-Scale Structures Group, Institut Laue-Langevin, 38000 Grenoble, France

Edited by Gregory A. Petsko, Brigham and Women's Hospital, Boston, MA, and approved February 12, 2020 (received for review November 8, 2019)

In redox metalloenzymes, the process of electron transfer often involves the concerted movement of a proton. These processes are referred to as proton-coupled electron transfer, and they underpin a wide variety of biological processes, including respiration, energy conversion, photosynthesis, and metalloenzyme catalysis. The mechanisms of proton delivery are incompletely understood, in part due to an absence of information on exact proton locations and hydrogen bonding structures in a bona fide metalloenzyme proton pathway. Here, we present a 2.1-Å neutron crystal structure of the complex formed between a redox metalloenzyme (ascorbate peroxidase) and its reducing substrate (ascorbate). In the neutron structure of the complex, the protonation states of the electron/proton donor (ascorbate) and all of the residues involved in the electron/proton transfer pathway are directly observed. This information sheds light on possible proton movements during heme-catalyzed oxygen activation, as well as on ascorbate oxidation.

heme | neutron | peroxidase | ascorbate | proton transfer

In biological systems, the movement of an electron (or electrons) is commonly accompanied by the movement of a proton (or protons). These proton-coupled electron transfer (PCET) reactions, carried out by redox-active metalloproteins, are related in concept to the more simplistic hydrogen atom transfer ($H^{\bullet}$ transfer) mechanisms that have been studied in organic chemistry for much longer, since a hydrogen atom can be considered as merely a proton and an electron conjoined (1, 2). However, the mechanisms of how proton transfer is coupled to electron transfer in biology are incompletely understood. One of the limitations has been that the (hydrogen bonding) pathways for delivery of protons through a metalloprotein matrix are, on the whole, poorly defined; and in cases where possible proton delivery pathways have been defined at a structural level in X-ray crystallographic work—for example in cytochrome *c* oxidase, nitric oxide reductase, or cytochrome P450 (3–7)—the locations of protons on individual amino acids in the proton pathway(s) have not. Neutron crystallography, in contrast, has the capability to visualize and assign the locations of hydrogen (deuterium) atoms, and thus has the potential to unravel the details of proton transfer pathways.

Ascorbic acid (Vitamin C) is a widely used biological reductant, and its redox chemistry (Scheme 1) involves transfer of an electron and a proton. The heme enzyme ascorbate peroxidase (APX) catalyzes the H_2O_2-dependent oxidation of ascorbate (2 ascorbate + H_2O_2 → 2 monodehydroascorbate + 2 H_2O). Cytosolic APXs are a member of the wider heme peroxidase family and, like the closely related cytochrome *c* peroxidase enzyme, they are classified as class I peroxidases (8). For APX, the mechanism of ascorbate oxidation proceeds by means of a two-equivalent oxidized ferryl intermediate of the heme, known as compound I, which is the same intermediate as is used in all other peroxidases that oxidize different kinds of substrates. Since the reduction of hydrogen peroxide (O_2^{2-}) to water (O^{2-}) is a two-electron process, then in electron counting terms compound I can be formally considered as a Fe^{V} species (i.e., two equivalents above the ferric resting state). However, Fe^{V} is never observed in heme species, and instead compound I is always found as an Fe^{IV} ferryl with either a porphyrin pi-cation radical (e.g., in APX and most other peroxidases) or a tryptophan radical (e.g., in cytochrome *c* peroxidase) (9). This compound I species abstracts a hydrogen atom ($H^{\bullet}$) from ascorbate (HS) in two sequential single-electron reduction steps that involve the formation of a second intermediate called compound II, which contains only the Fe^{IV} species and not the radical (**Eqs. 1–3**):

$$\text{APX} + \text{H}_2\text{O}_2 \rightarrow \text{Compound I} + \text{H}_2\text{O}, \quad [1]$$

$$\text{Compound I} + \text{HS} \rightarrow \text{Compound II} + \text{S}^{\bullet}, \quad [2]$$

$$\text{Compound II} + \text{HS} \rightarrow \text{APX} + \text{S}^{\bullet} + \text{H}_2\text{O}. \quad [3]$$

As with other enzyme-catalyzed oxidations of ascorbate, the APX mechanism is formally considered as transfer of an electron

Significance

The simultaneous transfer of a proton and an electron—a process that is referred to as proton-coupled electron transfer (PCET)—is ubiquitous in biology. Many redox metalloenzymes that are used for electron transfer also require proton transfer, making PCET a fundamental component of metalloenzyme catalysis. We present a neutron crystal structure for an enzymatic PCET pathway in the heme enzyme ascorbate peroxidase. The protonation state of the proton/electron donor (ascorbate) is observed bound to the enzyme, and the locations of the deuterium atoms on the proton transfer pathway are directly visualized. This atomic map of a biological proton transfer pathway provides a framework for understanding proton delivery processes in other heme enzymes.

Author contributions: M.W.v.d.K., A.J.M., M.P.B., P.C.E.M., and E.L.R. designed research; H.K., J.B., J.M.D., R.S., M.W.v.d.K., T.E.S., A.O., M.P.B., and P.C.E.M. performed research; H.K., J.B., J.M.D., R.S., M.W.v.d.K., A.J.M., T.E.S., A.O., M.P.B., P.C.E.M., and E.L.R. analyzed data; and P.C.E.M. and E.L.R. wrote the paper.

The authors declare no competing interest.

This article is a PNAS Direct Submission.

Data deposition: Atomic coordinates have been deposited in the Protein Data Bank, https://www.wwpdb.org (PDB ID codes 6XV4 [APX–ascorbate complex] and 6TAE [ferric APX]).

[1]To whom correspondence may be addressed. Email: peter.moody@le.ac.uk or emma.raven@bristol.ac.uk.

This article contains supporting information online at https://www.pnas.org/lookup/suppl/doi:10.1073/pnas.1918936117/-/DCSupplemental.

First published March 9, 2020.

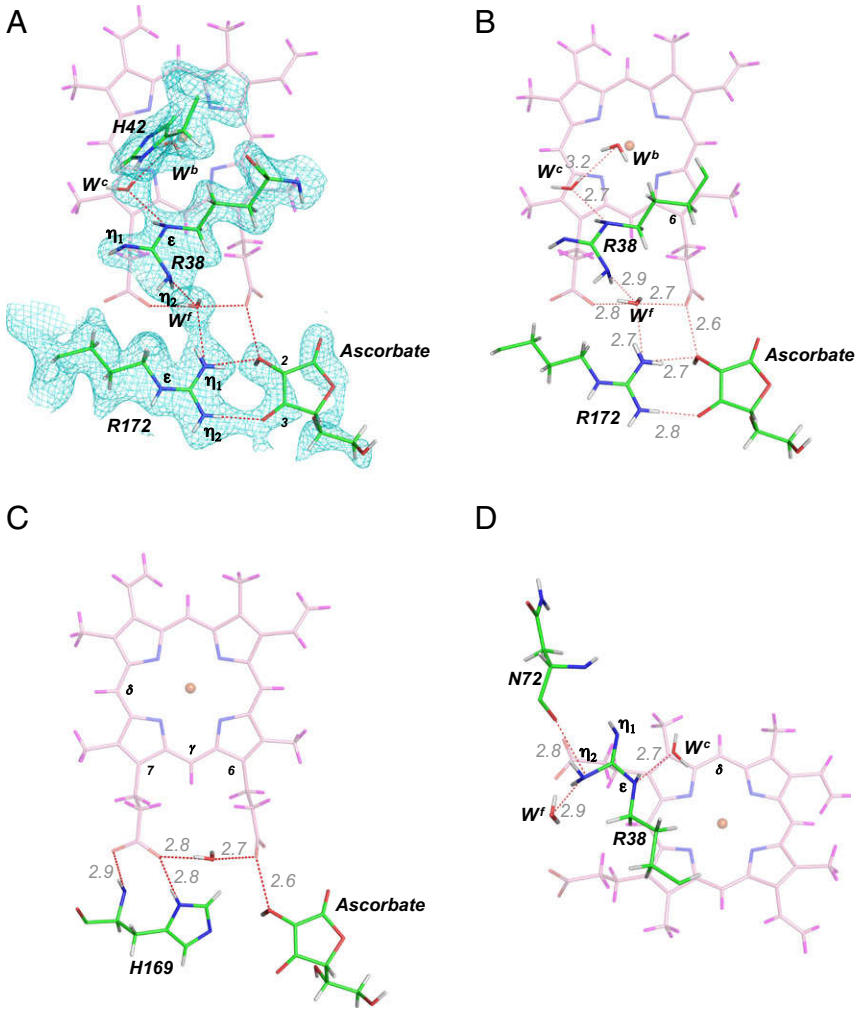

Fig. 1. (*A*) The neutron structure of the ascorbate peroxidase (APX)–ascorbate electron transfer complex. Nuclear density ($2F_o - F_c$) of Arg38, His42, Arg172, and ascorbate is shown in cyan (contoured at 1.5σ). For simplicity, the heme is shown in pink and at partial transparency with the hydrogen atoms shown in magenta, oxygen atoms in red, nitrogen atoms in blue, deuterium in white, and carbon in green. Arg38 is in the neutral (guanidine) form. Water molecules are indicated as W; waters *b* (W^b) and *c* (W^c) that are included in the mechanism in Fig. 3 are labeled accordingly. (*B*) Skeleton outline of the proton transfer pathway, highlighting only the individual deuterium atoms and hydrogen bonds involved. (*C*) The hydrogen bonding arrangements in the region of the heme 6-propionate and 7-propionates (labeled 6 and 7, respectively) and His169. (*D*) The local environment of the Arg38 residue, showing the hydrogen bonding interactions between the guanidine group and Asn72 and water molecules that are within hydrogen bonding distance of Arg38. A further water molecule (W^f) is identified (shown also Figs. 3 and 4). The δ- and γ-heme edges are labeled for reference in *C* and *D*. Hydrogen bond distances (in angstroms) are shown in gray in *B*–*D*. Because of the rotational freedom of the water molecules, only the distances between hydrogen bond donor and acceptor are shown.

and the simultaneous (concerted) movement of a proton (9); because of this, it has been used as a framework for the more general understanding of biological processes that depend on ascorbate (1). Here, we present a neutron crystal structure for the electron transfer complex formed between ascorbate and APX enzyme. In the neutron structure of the complex, the protonation state of the bound ascorbate and of all of the residues involved in the electron/proton transfer pathway are directly visualized.

Results

Hydrogen atoms scatter X-rays very weakly and thus are difficult to detect in electron density maps. In contrast, in a neutron crystallography experiment, neutrons are scattered strongly, albeit negatively (scattering length, −3.74 fm), by hydrogen atoms and thus become visible at lower resolutions than required with X-rays (10). The substitution of (exchangeable) hydrogen atoms with its isotope deuterium (scattering length, +6.67 fm) leads to improvements in the diffraction data as incoherent scattering from hydrogen atoms is reduced (11). Perdeuteration of protein samples—where all (not just the exchangeable) hydrogen atoms are replaced with deuterium—gives further improved assignments of proton locations. Neutron crystallography, therefore, has the capability to directly observe the locations of individual hydrogen (deuterium) atoms, and thus has the potential to unravel the details of proton transfer pathways.

The neutron crystal structure of perdeuterated (i.e., fully deuterated; see *Materials and Methods*) ferric APX in complex with ascorbate was obtained at 2.1-Å resolution and was jointly refined with X-ray diffraction data at 1.9-Å resolution. A 2.2-Å resolution neutron structure of perdeuterated ferric APX in the absence of ascorbate was also obtained. Both neutron structures (250 residues) show a mainly α-helical structure with a heme group at the core. Data collection and refinement statistics for both structures are given in *SI Appendix*, Table S1, for

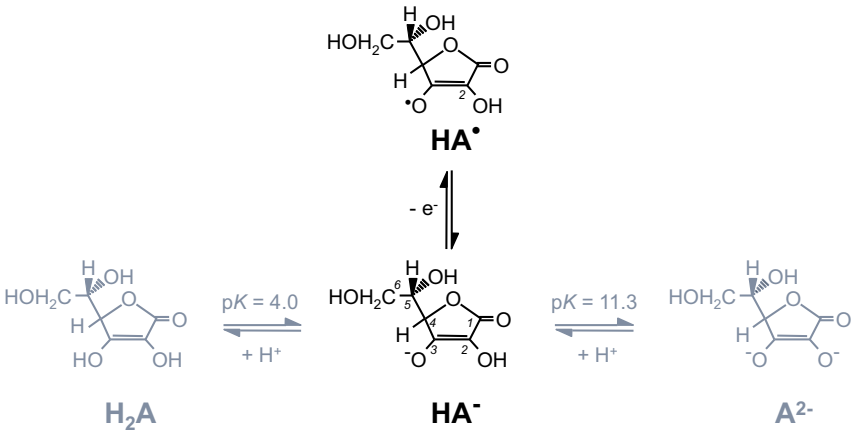

Scheme 1. Scheme showing the chemistry of ascorbate. In the physiological pH range (shown in black), ascorbate exists as a singly deprotonated form (HA^-). One electron oxidation formally leads to formation of the monodehydroascorbate radical ($HA^•$), which is highly acidic [$pK_a = -0.45$ for the OH group on C^2 (52)] and releases a proton. Thus, the oxidation of ascorbate (HA^-) formally involves one electron and one proton (and overall one $H^•$). Other forms of ascorbate, which exist outside of the normal biological pH range, are indicated in gray.

both the neutron and X-ray datasets. Nuclear scattering density of the ferric APX–ascorbate complex in the region of the heme and the bound ascorbate is shown in Fig. 1*A*; the hydrogen bonding interactions alone are indicated in Fig. 1*B*. In both structures, a water molecule (labeled W^b in Fig. 1) is located above the iron on the distal side (Fig. 1 and *SI Appendix*, Fig. S1). The bond lengths to water are similar (Fe–O = 2.24 Å in the ferric APX–ascorbate complex; Fe–O = 2.33 Å in ferric APX); this is within bonding range, although in solution APX likely exists as a mixture of mainly 5-coordinate heme in equilibrium with some 6-coordinate, water-bound species. The protonation states of all active-site residues and of the heme group itself are visible in the neutron structure and are shown for the ferric APX–ascorbate complex and for ferric APX (*SI Appendix*, Fig. S1). Note that His42 is neutral in both ferric structures, as it is in the closely related ferric cytochrome *c* peroxidase structure (12). The bound ascorbate is deuterated on C^2, but not on C^3, and is thus found as the singly deprotonated state (HA^-, Scheme 1). Arg172 hydrogen bonds to the ascorbate and is observed in the fully protonated (guanidinium) form, with the nitrogen atoms on both $N\eta_1$ and $N\eta_2$ each carrying two deuterium atoms (i.e., present as ND_2 on both the η_1 and η_2 atoms in Arg172) (Fig. 1 *A* and *B*). The OD group of the bound ascorbate also hydrogen bonds to the 6-propionate of the heme (Fig. 1 *B* and *C*). Other hydrogen bonding interactions in the region of the 6- and 7-propionates are shown in Fig. 1*C*.

In the neutron structure of the ferric APX–ascorbate complex, all of the deuterium atoms can be defined in a proton transfer pathway that leads from the substrate to the heme and involves Arg38, Arg172, and three water molecules (W^f, W^c, and W^b) (Fig. 1*B*). In this pathway, a series of hydrogen bonds and the locations of deuterium atoms on all of the residues have been identified. The nuclear density map shows that Arg38 is singly deuterated on $N\eta_1$ (i.e., present as ND on the η_1 atom) and doubly deuterated on $N\eta_2$ (i.e., present as ND_2 on the η_2 atom) (Fig. 2*A*). Arg38 is thus interpreted as being present in a neutral (guanidine) form in the ferric APX–ascorbate complex. The local hydrogen bonding environment around this Arg38 residue is shown in Fig. 1*D*. Difference (omit) maps and occupancy refinements were used to test the interpretation of the deuterium atom positions in Arg38 (*SI Appendix*, Fig. S2). The shape and positions of the difference map indicates that only one deuterium, on $N\eta_1$, is missing; this is consistent with the assignment of a neutral Arg. The structure of Arg38 observed in our experiments is in agreement with structures of neutral Arg residues drawn in organic chemistry (13), although in principle four other tautomeric forms are possible [corresponding to loss of each of the remaining four nitrogen-bound protons (14)]. Both the nuclear (Fig. 2*A*) and electron density maps are consistent with the change from a planar guanidinium side chain in the (fully delocalized) charged state to tetrahedral geometry at Nε and $N\eta_2$ as expected for the neutral form with a double bond between Cζ and $N\eta_1$. In solution, the five tautomeric forms are expected to interconvert (15) in a pH-independent equilibrium by means of bond rotations and/or proton transfer, and note that a different tautomeric form of neutral Arg has been observed in T4 lysozyme (16). By comparison, in the corresponding neutron map of the (ascorbate-free) ferric APX enzyme (Fig. 2*B* and *SI Appendix*, Fig. S1), Arg38 is interpreted as positively charged and existing

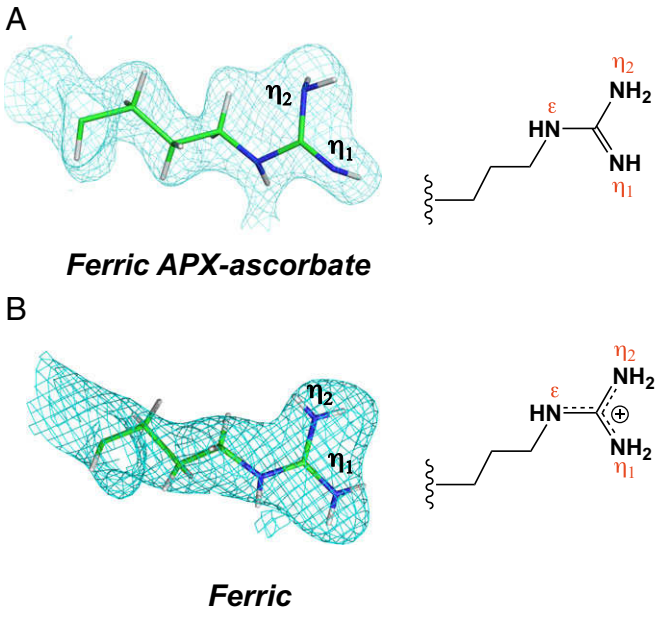

Fig. 2. Nuclear density ($2F_o - F_c$), shown in cyan and contoured at 1.5σ for Arg38 in (*A*) the ferric APX–ascorbate complex and (*B*) ferric APX structure.

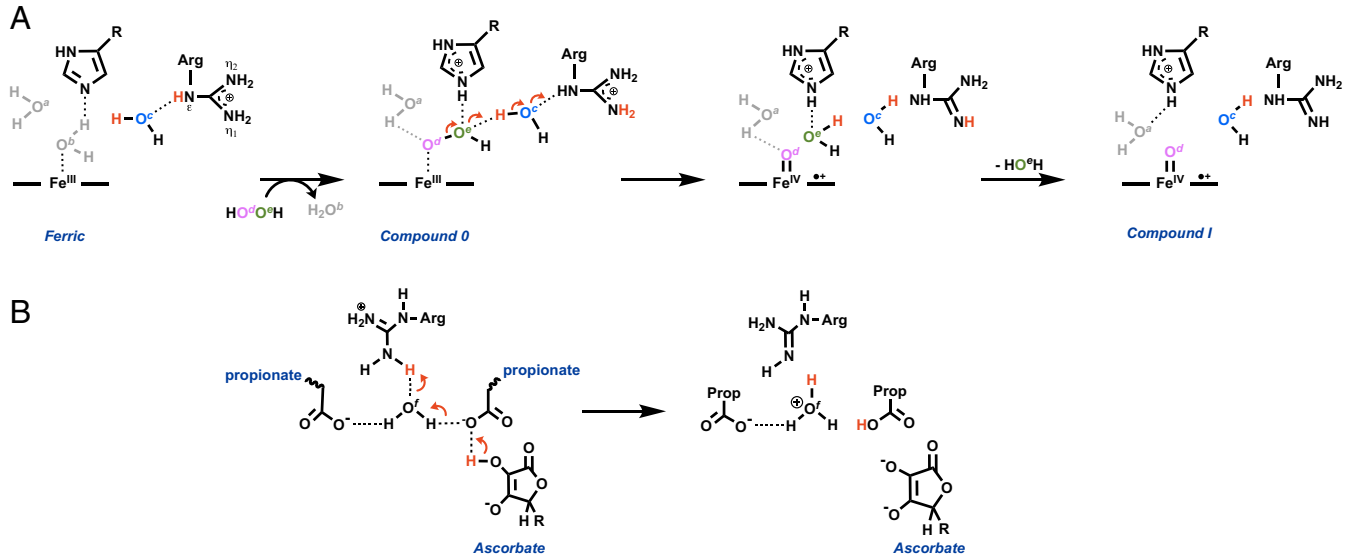

Fig. 3. Exemplars of possible movements of protons involving Arg38, based on an analysis of neutron structures for ferric APX and the ferric APX–ascorbate complex and on the neutron structure of compound II of APX (53). In *A* is envisaged a series of proton transfers that occur during O–O bond cleavage and formation of compound I. Note that the distal Arg and the water molecule labeled *c* (in blue) swap positions between APX (shown here) and CcP (12) (the latter having Arg48 in the position of water *c*), which may open up alternative proton delivery pathways (see text). In *B* is envisaged proton delivery from the H• donor (ascorbate) to Arg38 during reduction of compounds I or II. Since tautomeric forms of Arg will rapidly interconvert in solution, other combinations of proton movements are possible; this could include using neutral arginine as a catalytic base, to act as the "pull" for the concerted movement of protons from one place to another during different parts of a catalytic cycle [as previously suggested (29)]. Note also that His42 is unprotonated in both ferric APX structures (*SI Appendix*, Fig. S1); this is analogous to the equivalent His52 residue in CcP (12), which is also neutral. Proton delivery to the distal histidine is presumed in the mechanism here, as both His42 in APX (53) and His52 in CcP (12) are protonated after reaction with H_2O_2. Individual water molecules are labeled as *a*–*f* and colored accordingly; the structural positions of water molecules *a*–*c* and *f* are indicated in Fig. 1 and *SI Appendix*, Fig. S1. The proposed structure shown for compound 0 is the same as that identified by computation (54) and the proposed hydrogen bond identified computationally shown in gray.

in the protonated (guanidinium) form (i.e., doubly deuterated on both $N\eta_1$ and $N\eta_2$).

To further investigate the structure, and to examine the validity of potential proton transfer pathways, we performed multiple molecular dynamics simulations. These showed an ordered active site, consistent with the neutron structure, with defined positions of water molecules within it (*SI Appendix*, Fig. S3). Water molecules in the active site are positioned such that they can form a viable proton transfer chain between Arg38 and the heme iron as well as between Arg38 and ascorbate (via a propionate group).

Discussion

The locations of protons are not usually visible in X-ray structures, which makes the process of identifying protons and proton delivery mechanisms in metalloenzymes imprecise. In a neutron experiment, however, deuterium atoms appear in the maps with similar nuclear density (coherent scattering length, +6.67 fm) as carbon (+6.65 fm) and oxygen (+5.80 fm). This means that, at moderate resolution, the positions of all deuterium atoms can be confidently assigned. We have used this approach to produce an atomic map of the proton transfer pathway in the ascorbate–APX complex.

Beginning with a discussion of the nature of the ascorbate itself, a significant observation is that the positions of the deuterium atoms in the bound ascorbate (Fig. 1) show ascorbate present as an anionic species (HA^- in Scheme 1), which is consistent with its role as an H• (i.e., H^+ and e^-) donor. This is expected according to the chemistry of ascorbate but has not previously been confirmed in an enzyme–substrate complex. The 6-propionate forms a hydrogen bond to the anionic ascorbate and, in doing so, provides stabilization for the bound substrate alongside a presumed but plausible pathway for electron transfer from the substrate to the heme. It has been suggested that the heme propionates could represent a general route for delivery of electrons in and out of heme proteins (17). As we discuss below, an involvement of the heme propionate in proton delivery is now also identified.

Moving on to a consideration of biological ascorbate oxidation, proton delivery is believed to occur as a concerted process, involving the simultaneous movement of an electron and a proton (1). For APX-catalyzed ascorbate oxidation in particular, concerted (and rate-limiting) movement of several protons along a pathway from ascorbate to the ferryl oxygen of the heme is envisaged (18). The active-site Arg38 is believed to be intrinsic to the PCET pathway (19, 20). In our neutron maps, Arg38 is observed in the neutral (guanidine) form in the presence of ascorbate. There is no obvious feature of the Arg38 local environment (Fig. 1*D*) that would favor deprotonation, and a large decrease from the estimated pK_a in solution [$pK_a \sim 13$ (15, 21)] would be required. In our analyses of other arginine residues in APX and in the closely related cytochrome *c* peroxidase (CcP) enzyme (12), we have not identified examples of neutral guanidine groups in any other cases, which makes Arg38 in the ferric APX–ascorbate complex stand out. That is not to imply that Arg38 is stable as a neutral species in the substrate-bound or any other form of the enzyme in solution, as the particular crystallization conditions used in our experiment may have led to "trapping" of Arg38 in a neutral state. Our view instead is that Arg38 is known to be mobile (22), which is presumed to assist in proton shuttling; that its removal is known to directly impose upon the proton delivery event (18); and that these features are consistent with the need for Arg38 to switch transiently between neutral and charged states as the enzyme cycles through different intermediates in the catalytic mechanism. There are other crystallographically defined redox metalloenzymes in which

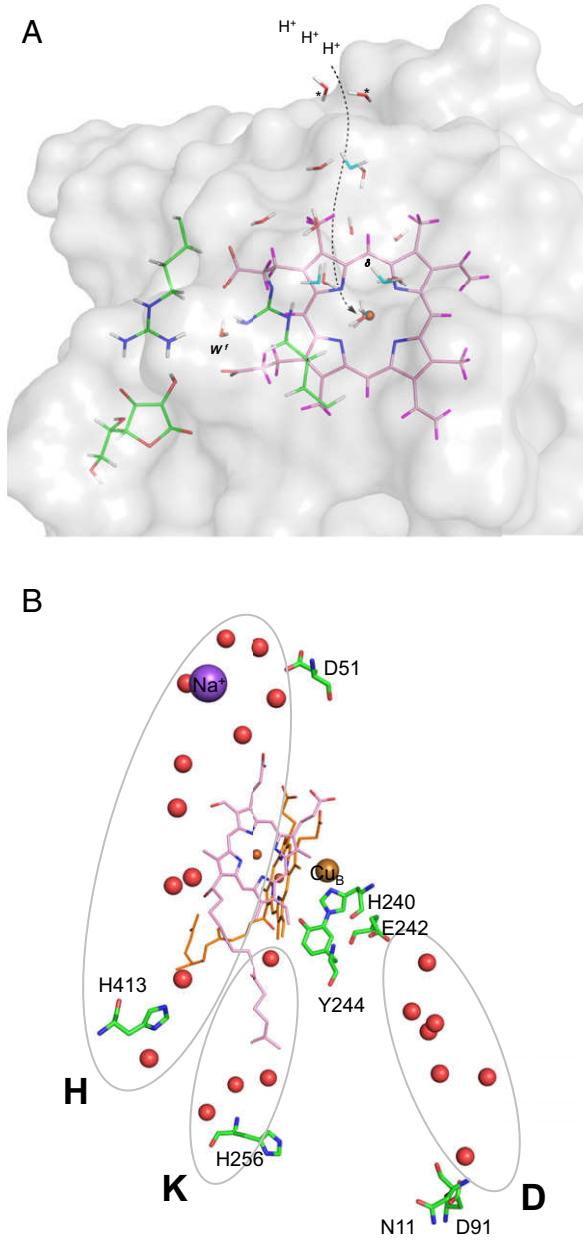

Fig. 4. Comparison of possible proton channels. (*A*) The figure shows a channel of water molecules extending out from the heme in the direction of the δ-heme edge in the ferric APX–ascorbate complex, which may function as an alternative proton delivery pathway. The waters are positioned within hydrogen-bonding range of one another (~2.8 Å), with the exception of the two outer waters (labeled *), which are ~3.8 Å from their adjacent waters. The distance between the iron of the heme group and the two outer waters is ~12.4 Å. Our expectation is that water molecules move slightly and are not static in solution, as is evidenced by the fact that the water positions in the ferric APX–ascorbate complex (shown in red for oxygen and white for deuterium) are slightly altered from those in the ferric-only structure (overlaid in cyan/white). Compare also the slightly different orientations of conserved water molecules (*SI Appendix*, Fig. S1 *A* and *B*). The color scheme is the same as that shown in Fig. 1. (*B*) For comparison, the schematic shows proposed proton transfer pathways (H, K, and D channels) in bovine heart cytochrome *c* oxidase [PDB ID code 5B1A (55)]. The D channel connects D91 to E242; the K channel connects to Y244; and the H channel connects to D51 via the pyrrole of heme (redrawn from ref. 56). Water molecules identified in the crystal structure are shown as red spheres.

arginine residues are implicated as proton shuttles in a pathway (6, 18, 23–29), and this also, by necessity, presumes an ability of arginine to deprotonate. We note here that evidence exists for neutral Arg residues identified in other neutron structures (16, 30–32), and the concept of a (neutral) arginine acting as a base in metalloenzyme-catalyzed proton transfer reactions has been put forward (29).

Thinking more generally about how protons wend their way through a pathway, we emphasize that while a neutron experiment on a single enzyme state can identify the locations of deuterium atoms it cannot identify their origin. Thus, it is not possible to assign individual protons (e.g., on an arginine) in a single enzyme state as arising from an individual proton donor (e.g., from ascorbate), as there are many sources of protons in rapid solvent exchange within an enzyme active site. Because of this, it is not possible to monitor movements of individual protons. That said, it is valid to use the information obtained from neutron structures to speculate on possible proton delivery mechanisms through a defined pathway. We have done so in Fig. 3, by showing possible proton movements involving Arg38 in APX. Since there is now good evidence that the distal histidine (His42) also changes protonation state during catalysis (12), movements of protons on and off these two residues within the active site would form the basis for an overall proton relay mechanism and would provide convenient repositories for protons at different stages of the catalytic cycle.

Further examination of the neutron structures shows that ascorbate may not be the only source of protons into the peroxidase active site. For extending outwards, in the direction of the δ-heme edge, lies a chain of water molecules that reach as far as the surface of the molecule (Fig. 4*A*). This pattern of water molecules resembles the proton channels that have been proposed previously in the proton-pumping cytochrome *c* oxidase enzyme (33–35) (Fig. 4*B*). In cytochrome *c* oxidase, there are three proposed proton channels (D, H, and K). We note that the water–water distances in some cases are as much as 8 Å in the H and K channels, and ~4 to 5 Å in the D channel, which we interpret to mean that the proton channels are not affected by large gaps between each water molecule. Similarly, the individual orientations of these water molecules in APX do not allow us to identify a completely unbroken chain of waters with each hydrogen bonded to the next, and there are gaps in some places (Fig. 4*A*). However, individual water molecules have rotational freedom and are likely to adjust slightly in both location and orientation during the mechanism, and there is evidence for this when comparing water molecule positions in different structures (as is shown for example in Fig. 4*A*). It is therefore feasible, taking into account suitable small adjustments of water molecule positions, that the pathway depicted in Fig. 4*A* could provide an alternative continuous conduit for protons migrating into the active site. Such complex interplays of proton movements involving substrates, water molecules, and titratable amino acids are relevant to the understanding of catalytic oxygen activations events in other heme proteins (36, 37), including those enzymes that use ascorbate (38).

Materials and Methods

Protein Expression and Purification. Soybean cytosolic APX in a pLEICS-03 vector was expressed in *Escherichia coli* BL21 (DE3) cells. Cells were grown in 2× YT media for 16 h at 37 °C without induction. Cells were harvested, and APX was purified as previously described (8, 39, 40). Purified samples were concentrated, and then diluted 20 times with 10 mM potassium phosphate, pH 7.0, made up in D_2O. Samples were incubated overnight at 4 °C to allow exchange of hydrogens with deuterium.

Deuteration. To obtain perdeuterated APX protein, a high-cell density fermentation process was carried out in the Deuteration Laboratory of the Institut Laue-Langevin (ILL) (Grenoble, France). The pLEICS-03 vector containing cDNA coding for soybean APX was transformed into Rosetta (DE3)

cells (Novagen). Cells were adapted to deuterated ENFORS minimal medium (41) in the presence of kanamycin and chloramphenicol, each at a final concentration of 35 μg/mL. Cells were grown using a fed-batch fermentation strategy in minimal medium with d_8-glycerol (99% deuterium; Euriso-top) as carbon source and D_2O as solvent. The bacteria were grown at 30 °C to an OD_{600} of 11 to 12, the temperature was then decreased to 28 °C, and protein expression was induced by addition of isopropyl β-D-1-thiogalactopyranoside to a final concentration of 1 mM. Bacteria were harvested by centrifugation when an OD_{600} of 16 to 20 was reached, after 18 to 19 h of induction at 28 °C. Perdeuterated APX prepared in this way was purified and crystallized as mentioned above for the nonperdeuterated protein, using H_2O-based buffers.

Crystallization. Crystals of ferric APX were grown by vapor diffusion in hanging drops made up of 2 to 4 μL of protein (20 mg/mL in 10 mM potassium phosphate, pH 7.0, 150 mM KCl made with D_2O) and an equal volume of precipitant (2.25 M Li_2SO_4, 0.1 M Hepes, pH 8.3 to 8.9 made with D_2O). The drop was allowed to equilibrate with 700 μL of precipitant. Crystals appeared in 2 to 14 d. Once the crystals were fully grown, the crystals were transferred and kept in the mother liquor with D_2O until needed. Formation of the ferric APX–ascorbate complex was achieved by soaking the APX crystals in 50 mM ascorbate solution made with D_2O mother liquor for 10 min at 4 °C and then cryocooling crystals in liquid nitrogen. Successful formation of the complex was confirmed by X-ray crystallography. The ferric APX–ascorbate complex is stable and noncatalytic in the absence of peroxide (42).

X-Ray Data Collection. The X-ray structure of the ferric APX–ascorbate complex was solved by merging the first 10° of data from 10 different crystals to avoid photoreduction effects in the X-ray beam. The datasets were collected in-house at 100 K using CuKα radiation (λ = 1.5418 Å) from a Rigaku MicroMax 007HF generator. Crystals of ferric APX soaked with ascorbate as above and 20 images of 0.5° oscillation with 1-s exposure per image were recorded on a Rigaku Saturn 944+ detector to a resolution of 1.8 Å from each crystal. Data were indexed using iMOSFLM (43), and then scaled and merged using AIMLESS as part of the CCP4 suite (44). The statistics for the X-ray data collection are shown in *SI Appendix*, Table S1.

Neutron Data Collection of Ferric APX. Data were collected on a perdeuterated APX crystal at the LADI-III beamline at ILL (Grenoble, France). For data collection, cold neutrons with wavelengths from 2.87 to 3.4 Å were used. Quasi-Laue neutron diffraction data extending to 2.2-Å resolution were collected at 100 K. The neutron data were processed using the program LAUEGEN modified to account for the cylindrical geometry of the detector (45). The program LSCALE (46) was used to determine the wavelength-normalization curve using the intensities of symmetry-equivalent reflections measured at different wavelengths. No explicit absorption corrections were applied. These data were then merged in SCALA (44). The statistics for the neutron data collection are shown in *SI Appendix*, Table S1.

Neutron Data Collection of Ferric APX–Ascorbate Complex. Data were collected at the BIODIFF beamline at the Forschungsreaktor München II (FRM II) research reactor. A large single crystal of perdeuterated APX was soaked with ascorbate as above, to form the APX–ascorbate complex, and was then directly cryocooled to 100 K in a N_2 gas cryostream and stored in liquid nitrogen prior to data collection. Monochromatic neutron diffraction data were collected to 2.1-Å resolution at 100 K. The diffraction data were indexed and integrated using HKL2000 v705b and scaled using SCALEPACK (47). The statistics for the neutron data collection are shown in *SI Appendix*, Table S1.

Joint Structure Refinement. For the ferric APX structure, crystals used for the data collection were isomorphous with the previously published APX X-ray structure (PDB ID code 1OAG). All solvent molecules and ligand were removed from 1OAG, which was then used as the starting model. For the ferric APX–ascorbate complex, the low-dose X-ray structure was solved and refined first, then used as a starting model for the structure of the APX–ascorbate complex. For both structures, the joint X-ray and neutron refinements were carried out with PHENIX (48). The restraints file for Arg38 was modified to accommodate the observed neutral guanidine form in the ferric APX–ascorbate complex. D_2O molecules were added based on a neutron $F_o - F_c$ map. The model building was completed with Crystallographic Object-Oriented Toolkit (COOT) software (49). Determination of the identity and the position of heme ligand were based on neutron data only. Joint X-ray/neutron structural refinement statistics are given in *SI Appendix*, Table S1. Atomic coordinates have been deposited in the Protein Data Bank under the ID codes 6XV4 (APX–ascorbate complex) and 6TAE (ferric APX).

Computational Methods. Molecular dynamics simulations were performed using NAMD (50) and the CHARMM36 forcefield (51) with additional parameters as described in *SI Appendix*.

ACKNOWLEDGMENTS. We acknowledge beam time allocation, awarded from the BIODIFF beamline at FRM II and the LADI-III at ILL. This work was funded by Biotechnology and Biological Sciences Research Council (Grants BB/N015940/1 to P.C.E.M. and E.L.R., and BB/M026280/1 to M.W.v.d.K.) and the Engineering and Physical Sciences Research Council through the UK Catalysis Hub (Grant EP/M013219/1 to R.S., M.W.v.d.K., and A.J.M.). Computational resources were provided by the Advanced Computing Research Centre, University of Bristol (http://www.bristol.ac.uk/acrc), and the ARCHER UK National Supercomputing Service (http://www.archer.ac.uk) via HECBioSim (Grant EP/L000253/1). We are grateful to an anonymous reviewer for pointing out possible comparisons with other proton channels, and to Peter Rich (University College London) for helpful discussions on cytochrome *c* oxidase.

1. J. J. Warren, T. A. Tronic, J. M. Mayer, Thermochemistry of proton-coupled electron transfer reagents and its implications. *Chem. Rev.* **110**, 6961–7001 (2010).
2. G. A. Parada *et al.*, Concerted proton-electron transfer reactions in the Marcus inverted region. *Science* **364**, 471–475 (2019).
3. T. Tsukihara *et al.*, The whole structure of the 13-subunit oxidized cytochrome *c* oxidase at 2.8 Å. *Science* **272**, 1136–1144 (1996).
4. S. Iwata, C. Ostermeier, B. Ludwig, H. Michel, Structure at 2.8 Å resolution of cytochrome *c* oxidase from *Paracoccus denitrificans*. *Nature* **376**, 660–669 (1995).
5. S. Buschmann *et al.*, The structure of cbb3 cytochrome oxidase provides insights into proton pumping. *Science* **329**, 327–330 (2010).
6. T. Hino *et al.*, Structural basis of biological N_2O generation by bacterial nitric oxide reductase. *Science* **330**, 1666–1670 (2010).
7. I. Schlichting *et al.*, The catalytic pathway of cytochrome p450cam at atomic resolution. *Science* **287**, 1615–1622 (2000).
8. D. K. Jones, D. A. Dalton, F. I. Rosell, E. L. Raven, Class I heme peroxidases: Characterization of soybean ascorbate peroxidase. *Arch. Biochem. Biophys.* **360**, 173–178 (1998).
9. P. C. E. Moody, E. L. Raven, The nature and reactivity of ferryl heme in compounds I and II. *Acc. Chem. Res.* **51**, 427–435 (2018).
10. M. P. Blakeley, A. D. Podjarny, Neutron macromolecular crystallography. *Emerging Top. Life Sci.* **2**, 39–55 (2018).
11. S. J. Fisher *et al.*, Perdeuteration: Improved visualization of solvent structure in neutron macromolecular crystallography. *Acta Crystallogr. D Biol. Crystallogr.* **70**, 3266–3272 (2014).
12. C. M. Casadei *et al.*, Heme enzymes. Neutron cryo-crystallography captures the protonation state of ferryl heme in a peroxidase. *Science* **345**, 193–197 (2014).
13. J. Clayden, N. Greeves, S. Warren, *Organic Chemistry* (Oxford University Press, New York, ed. 2, 2012).
14. E. D. Raczynska *et al.*, Consequences of proton transfer in guanidine. *J. Phys. Org. Chem.* **16**, 91–106 (2003).
15. C. A. Fitch, G. Platzer, M. Okon, B. E. Garcia-Moreno, L. P. McIntosh, Arginine: Its pK_a value revisited. *Protein Sci.* **24**, 752–761 (2015).
16. T. Hiromoto *et al.*, Neutron structure of the T26H mutant of T4 phage lysozyme provides insight into the catalytic activity of the mutant enzyme and how it differs from that of wild type. *Protein Sci.* **26**, 1953–1963 (2017).
17. V. Guallar, Heme electron transfer in peroxidases: The propionate e-pathway. *J. Phys. Chem. B* **112**, 13460–13464 (2008).
18. I. Efimov *et al.*, Proton delivery to ferryl heme in a heme peroxidase: Enzymatic use of the Grotthuss mechanism. *J. Am. Chem. Soc.* **133**, 15376–15383 (2011).
19. K. H. Sharp, M. Mewies, P. C. Moody, E. L. Raven, Crystal structure of the ascorbate peroxidase-ascorbate complex. *Nat. Struct. Biol.* **10**, 303–307 (2003).
20. K. H. Sharp, P. C. Moody, K. A. Brown, E. L. Raven, Crystal structure of the ascorbate peroxidase-salicylhydroxamic acid complex. *Biochemistry* **43**, 8644–8651 (2004).
21. M. J. Harms, J. L. Schlessman, G. R. Sue, B. García-Moreno, Arginine residues at internal positions in a protein are always charged. *Proc. Natl. Acad. Sci. U.S.A.* **108**, 18954–18959 (2011).
22. A. Gumiero, C. L. Metcalfe, A. R. Pearson, E. L. Raven, P. C. Moody, Nature of the ferryl heme in compounds I and II. *J. Biol. Chem.* **286**, 1260–1268 (2011).
23. H. Luecke, H. T. Richter, J. K. Lanyi, Proton transfer pathways in bacteriorhodopsin at 2.3 angstrom resolution. *Science* **280**, 1934–1937 (1998).
24. M. K. Doherty *et al.*, Identification of the active site acid/base catalyst in a bacterial fumarate reductase: A kinetic and crystallographic study. *Biochemistry* **39**, 10695–10701 (2000).
25. N. C. Gerber, S. G. Sligar, A role for Asp-251 in cytochrome P-450cam oxygen activation. *J. Biol. Chem.* **269**, 4260–4266 (1994).

26. A. V. Pisliakov, T. Hino, Y. Shiro, Y. Sugita, Molecular dynamics simulations reveal proton transfer pathways in cytochrome C-dependent nitric oxide reductase. *PLOS Comput. Biol.* **8**, e1002674 (2012).
27. D. A. Mills *et al*., An arginine to lysine mutation in the vicinity of the heme propionates affects the redox potentials of the hemes and associated electron and proton transfer in cytochrome *c* oxidase. *Biochemistry* **44**, 10457–10465 (2005).
28. K. L. Pankhurst *et al*., A proton delivery pathway in the soluble fumarate reductase from *Shewanella frigidimarina*. *J. Biol. Chem.* **281**, 20589–20597 (2006).
29. R. M. Evans *et al*., Mechanism of hydrogen activation by [NiFe] hydrogenases. *Nat. Chem. Biol.* **12**, 46–50 (2016).
30. K. Yonezawa *et al*., Neutron crystallography of photoactive yellow protein reveals unusual protonation state of Arg52 in the crystal. *Sci. Rep.* **7**, 9361 (2017).
31. S. Yamaguchi *et al*., Low-barrier hydrogen bond in photoactive yellow protein. *Proc. Natl. Acad. Sci. U.S.A.* **106**, 440–444 (2009).
32. Y. V. Guillén Schlippe, L. Hedstrom, A twisted base? The role of arginine in enzyme-catalyzed proton abstractions. *Arch. Biochem. Biophys.* **433**, 266–278 (2005).
33. K. Faxén, G. Gilderson, P. Adelroth, P. Brzezinski, A mechanistic principle for proton pumping by cytochrome c oxidase. *Nature* **437**, 286–289 (2005).
34. M. Wikström, K. Krab, V. Sharma, Oxygen activation and energy conservation by cytochrome *c* oxidase. *Chem. Rev.* **118**, 2469–2490 (2018).
35. A. Malkamäki, B. Meunier, M. Reidelbach, P. R. Rich, V. Sharma, The H channel is not a proton transfer path in yeast cytochrome *c* oxidase. *Biochim Biophys Acta Bioenerg* **1860**, 717–723 (2019).
36. B. Meunier, S. P. de Visser, S. Shaik, Mechanism of oxidation reactions catalyzed by cytochrome p450 enzymes. *Chem. Rev.* **104**, 3947–3980 (2004).
37. X. Huang, J. T. Groves, Oxygen activation and radical transformations in heme proteins and metalloporphyrins. *Chem. Rev.* **118**, 2491–2553 (2018).
38. P. Lu *et al*., Structure and mechanism of a eukaryotic transmembrane ascorbate-dependent oxidoreductase. *Proc. Natl. Acad. Sci. U.S.A.* **111**, 1813–1818 (2014).
39. S. K. Badyal *et al*., Conformational mobility in the active site of a heme peroxidase. *J. Biol. Chem.* **281**, 24512–24520 (2006).
40. I. K. Macdonald, S. K. Badyal, L. Ghamsari, P. C. Moody, E. L. Raven, Interaction of ascorbate peroxidase with substrates: A mechanistic and structural analysis. *Biochemistry* **45**, 7808–7817 (2006).
41. M. Haertlein *et al*., Biomolecular deuteration for neutron structural biology and dynamics. *Methods Enzymol.* **566**, 113–157 (2016).
42. A. P. Hill *et al*., Chemical, spectroscopic and structural investigation of the substrate-binding site in ascorbate peroxidase. *Eur. J. Biochem.* **248**, 347–354 (1997).
43. T. G. Battye, L. Kontogiannis, O. Johnson, H. R. Powell, A. G. Leslie, iMOSFLM: A new graphical interface for diffraction-image processing with MOSFLM. *Acta Crystallogr. D Biol. Crystallogr.* **67**, 271–281 (2011).
44. M. D. Winn *et al*., Overview of the CCP4 suite and current developments. *Acta Crystallogr. D Biol. Crystallogr.* **67**, 235–242 (2011).
45. J. W. Campbell, Q. Hao, M. M. Harding, N. D. Nguti, C. Wilkinson, LAUEGEN version 6.0 and INTLDM. *J. Appl. Crystallogr.* **31**, 496–502 (1998).
46. S. Arzt, J. W. Campbell, M. M. Harding, Q. Hao, J. R. Helliwell, LSCALE—The new normalization, scaling and absorption correction program in the Daresbury Laue software suite. *J. Appl. Crystallogr.* **32**, 554–562 (1999).
47. Z. Otwinowski, W. Minor, "Processing of X-ray diffraction data collected in oscillation mode" in *Methods in Enzymology* (Academic Press, 1997), vol. 276, pp. 307–326.
48. P. V. Afonine *et al*., Towards automated crystallographic structure refinement with phenix.refine. *Acta Crystallogr. D Biol. Crystallogr.* **68**, 352–367 (2012).
49. P. Emsley, B. Lohkamp, W. G. Scott, K. Cowtan, Features and development of Coot. *Acta Crystallogr. D Biol. Crystallogr.* **66**, 486–501 (2010).
50. J. C. Phillips *et al*., Scalable molecular dynamics with NAMD. *J. Comput. Chem.* **26**, 1781–1802 (2005).
51. J. Huang, A. D. MacKerell, Jr, CHARMM36 all-atom additive protein force field: Validation based on comparison to NMR data. *J. Comput. Chem.* **34**, 2135–2145 (2013).
52. D. M. Bryan *et al*., Stable pentaammineruthenium(III) complexes of reductic acids—synthesis, linkage isomers, and autoxidation kinetics. *J. Am. Chem. Soc.* **110**, 1498–1506 (1988).
53. H. Kwon *et al*., Direct visualization of a Fe(IV)-OH intermediate in a heme enzyme. *Nat. Commun.* **7**, 13445 (2016).
54. P. Vidossich *et al*., On the role of water in peroxidase catalysis: A theoretical investigation of HRP compound I formation. *J. Phys. Chem. B* **114**, 5161–5169 (2010).
55. N. Yano *et al*., The Mg^{2+}-containing water cluster of mammalian cytochrome *c* oxidase collects four pumping proton equivalents in each catalytic cycle. *J. Biol. Chem.* **291**, 23882–23894 (2016).
56. P. R. Rich, Mitochondrial cytochrome *c* oxidase: Catalysis, coupling and controversies. *Biochem. Soc. Trans.* **45**, 813–829 (2017).